On the dynamic mechanical properties of open-cell metal foams – A re-assessment of the 'simple-shock theory'

P.J. Tan [a,*], S.R. Reid [b], J.J. Harrigan [b]

[a] Department of Mechanical Engineering, University College London, Torrington Place, London WC1E 7JE, UK
[b] School of Engineering, University of Aberdeen, King's College, Aberdeen AB24 3UE, UK

ARTICLE INFO

ABSTRACT

Metal foams are increasingly used for energy absorption especially in lightweight structures and to resist blast and impact loads. This requires an understanding of the dynamic response of these materials for modelling purposes. As a supplement to Tan et al. (2005a,b), hereinafter referred to as *T–L* for brevity, this paper provides experimental data for the dynamic mechanical properties of open-cell Duocel® foams having a three-dimensional (3D) distribution of cells. These confirm significant enhancement of the foam's compressive strength, accompanied by changes in their deformation pattern in certain loading régimes, particularly what has come to be described as the 'shock' régime by Zheng et al. (2012). This paper examines experimentally, in a similar fashion as *T–L*, how the structural response of the individual cell walls is affected by cell-shape anisotropy at the cell (meso)-scale and how this, in turn, alters the pattern of cell crushing and the dynamic, mechanical properties. The distinctive role of cell microinertia and 'shock' formation are discussed in relation to the mechanical properties measured for these 3D cylindrical specimens. For consistency the same procedures described in *T–L* are used. The features identified are shown to be consistent with those observed in finite-element simulations of two-dimensional (2D) honeycombs as estimated by the one-dimensional (1D) steady-shock theory summarised in *T–L*. The different deformation patterns that develop in the various loading régimes are categorised according to the compression rate/impact speed. Critical values of impact velocity, corresponding to the transition from one pattern to the other, are quantified and predictive formulae for the compressive uniaxial strengths in the directions of two of the principal axes of the material in each loading régime are derived and discussed. The accuracy of the predictive formula in *T–L* is shown to critically depend on the 'densification strain' of the foam specimens. This parameter and the discussion that follows could assist the formulation and validation of alternative theoretical/computational models on the dynamic deformation of such materials.

© 2012 Elsevier Ltd. All rights reserved.

1. Introduction and motivation of study

To supplement previous work, exemplified by *T–L* and Zheng et al. (2012), this paper is concerned with an experimental investigation of Duocel® aluminium foam. Geometrically, Duocel® is a 3D open cell foam. Unlike its closed-cell counterpart, where compression of the cell fluid can lead to strain-rate dependence of the foam properties, the viscous contribution to the mechanical strength of open-cell foams is negligible even at high impact compression-rates because their large cell sizes – of the order of millimetres – allow gases to flow unimpeded through them (Gibson and Ashby, 1997). However, whilst the loading-rate sensitivity in the properties of open-cell foams might be attributed to rate sensitivity of the cell wall solid of which it was made, this loading rate

(or velocity–sensitivity) could be microinertial in origin, arising from the translational and rotational motions of the cell ligaments. This was discussed in the context of closed-cell Hydro/Cymat foams in *T–L*. The study reported herein is a supplement to the study in *T–L* and utilised Duocel® aluminium foam because of its more regular cell morphology. As well as providing validation data for future theoretical models, for metallic foams, the data enables a more critical assessment of various models in the literature to be explored.

In this paper, the experimental, dynamic mechanical properties of open-cell Duocel® foams are presented. The dynamic data were obtained using a 'direct-impact' technique. The analysis of the data is guided by results from finite-element simulations of the in-plane compression of simpler 2D honeycombs (Zou et al., 2009). That paper identified the internal mechanisms responsible for the deformation characteristics. The data, presented below and in *T–L*, indicate how the structural response of a 3D array of cells is influenced

* Corresponding author. Tel.: +44 0 20 7679 3754; fax: +44 0 20 7388 0180.
  E-mail address: pj.tan@ucl.ac.uk (P.J. Tan).

by the cell characteristics at the meso-scale and how this, in turn, alters the pattern of cell crushing and influences the dynamic mechanical properties measured. The subtle role of cell-shape anisotropy, hitherto a neglected topic, is also discussed.

These data enable a re-evaluation of the 'simple shock theory', first introduced in relation to the dynamic crushing of wood by Reid and Peng (1997) and presented, essentially, unchanged for metallic foams in T–L. Therein and others have utilised and extended this basic, simple, 'shock' model, for example Radford et al. (2005) and Zheng et al. (2012): however, it is now appropriate to re-evaluate some of the basic assumptions on which it was formulated, particularly in light of more recent advances.

Briefly, the literature on the dynamic mechanical properties of open-cell metal foams is still growing, some recent studies are given in Deshpande and Fleck (2000), Yi et al. (2001), Montanini (2005), Wang et al. (2006), Lee et al. (2006), Yu et al. (2006) and, more recently, in Elsinari et al. (2007) and Patofatto et al. (2007). However, as yet, there is no broad agreement on the details of the mechanism for the 'strain-rate', 'loading-rate' dependence or 'velocity-sensitivity' of the foam properties and the theoretical/ computational framework for modelling is. This paper is a contribution to this task. A common theme, that links the aforementioned studies, is the characterisation of the foams' dynamic properties (and/or the energy absorbed) in terms of a (suitably defined) nominal engineering stress-strain relationship, recognising the limitations of the definition of such a continuum concept for a cellular array with defined characteristic dimensions at the meso-scale.

As noted above, this paper is based on an experimental study of open-cell Duocel® foam, which has a more regular structure than the closed-cell foam used in the previous studies in T–L and should assist with elucidating a better understanding of the underlying deformation mechanisms.

2. Material description and topology of the Duocel® foam

Duocel® foams have a reticulated structure of open, duodeca-hedronal-shaped cells connected by continuous, solid ligaments made of the aluminium alloy Al6106–T6 which has a density (ρ_s) of 2700 kg m^{-3}, Young's modulus (E_s) of 70 GPa and yield strength (σ_{ys}) of 193 MPa. Each test specimen has nearly uniform density and suffers no obvious cell morphological defects except for minor variations in their cell size and cell-shape anisotropy with respect to the rise direction in the foaming process and transverse to this. These are denoted, respectively, by L and T below.

They were supplied by ERG as as-finished circular cylinders, cut with their axes in the L or the T directions. Unless stated otherwise the specimens had diameter d_o = 45 mm and gauge-length l_o = 50 mm. Each specimen had pore sizes of either 10 or 40 pores per inch (PPI), which corresponds to an average cell size of 4.0 mm and 2.0 mm respectively. The specimen dimensions were chosen so that the foam properties were not affected by cell size and gauge length effects (T–L). Some important parameters that characterise the Duocel® foams are listed in Table 1.

Anisotropy of the foam properties is due to cell elongation (see Fig. 1) resulting from the manufacturing process. Typical cell shape anisotropy ratios are listed in Table 1. To investigate the effects of cell shape anisotropy on the foam properties, specimens were supplied with either their smallest or largest principal cell dimension aligned to the loading axis. Hereinafter, the identifier 10T or 10L will be used to denote a 10PPI foam specimen compressed in the transverse (across the smallest cell dimension) or longitudinal (along the largest cell dimension) directions, respectively. Photographs of sectioned 10PPI specimens are shown in Fig. 1. Note that 40PPI-longitudinal (or 40L) specimens were only used in the

Table 1
Characterisation chart for Duocel® foams.

Commercial name	Duocel®	
Cell wall composition	Al6106–T6	
Density, ρ_0 (kg m^{-3})	257–287	210–271
Open or closed cells	Open	
Average cell diameter, $\bar{d}$ (mm)	4 (10 PPI)	2.0 (40 PPI)
Standard deviation of $\bar{d}$, $\mu_{\bar{d}}$ (mm)	0.2	0.07
Largest principal cell dimension, $\bar{L}_1$ (mm)	5.6	2.7
Smallest principal cell dimension, $\bar{L}_3$ (mm)	3.1	1.8
Intermediate principal cell dimension, $\bar{L}_2$ (mm)	4.1	2.1
Shape anisotropy ratios, R_{12}, R_{13}	R_{12} = 1.37	R_{12} = 1.29
	R_{13} = 1.81	R_{13} = 1.50

present study to permit the question of cell anisotropy to be explored more thoroughly.

3. Quasi-static compression

To appreciate fully the range of phenomena involved in the uniaxial compression of foams, their quasi-static compressive response was examined first. This also provides a reference point for subsequent discussions of the dynamic test data in Section 4.

3.1. Small engineering strain compressive response and cell deformation

The foams were compressed in a cylindrical chamber of 45 mm inner diameter to prevent their premature break-up by global buckling and/or shear banding – this imposes a uniaxial strain state in the specimen (T–L). It was found that the radial constraint had little effect on the pre-densification response of the foams; hence, it does not affect the foam properties to be discussed later as also confirmed by Radford et al. (2005).

Typical quasi-static, uniaxial, compressive stress-strain curves for the 10T, 10L and 40L specimens are given in Fig. 2. Note that stress and strain measures are based on engineering stress and nominal strain definitions. The use of these continuum concepts (particularly strain) are discussed in Reid and Peng (1997) and T–L. As with most cellular solids, they show linear elasticity at low stresses followed by a stress 'plateau' and a régime of densification in which the stress rises steeply (Gibson and Ashby, 1997). Their early compressive response, similar to that described by Bastawros et al. (2000) for closed-cell foams, can be delineated into three distinct phases as shown in Fig. 2(b). Phase 1 corresponds to linear, elastic straining of the cell ligaments during which the cells deform uniformly to a good approximation. Because the cells are initially more compliant in the transverse than the longitudinal direction, the elastic modulus in the latter is nearly twice the former which is consistent with the results of numerical simulations by Gong et al. (2005a,b). On further straining, the response becomes increasingly nonlinear as the deflection in the ligaments increases. This is identified as Phase 2.

Phase 3 responses in the longitudinal and transverse directions of the anisotropic foam are very different. In the former (10L and 40L specimens), localised microbuckling of the ligaments occur around small domains of spatially correlated defects which appear to spread and, eventually, coalesce to form bands of collapsing cells that advance across the specimen. When opposing cell walls in a collapsing band come into contact, the cells stiffen locally which triggers the collapse of a non-contiguous band of cells, with each band appearing to develop a spacing of 3–4 cell diameters with one another (Tan, 2005). This micro-buckling is particularly significant with respect to the deformation mechanisms under dynamic/ impact loading – see T–L and Section 4.
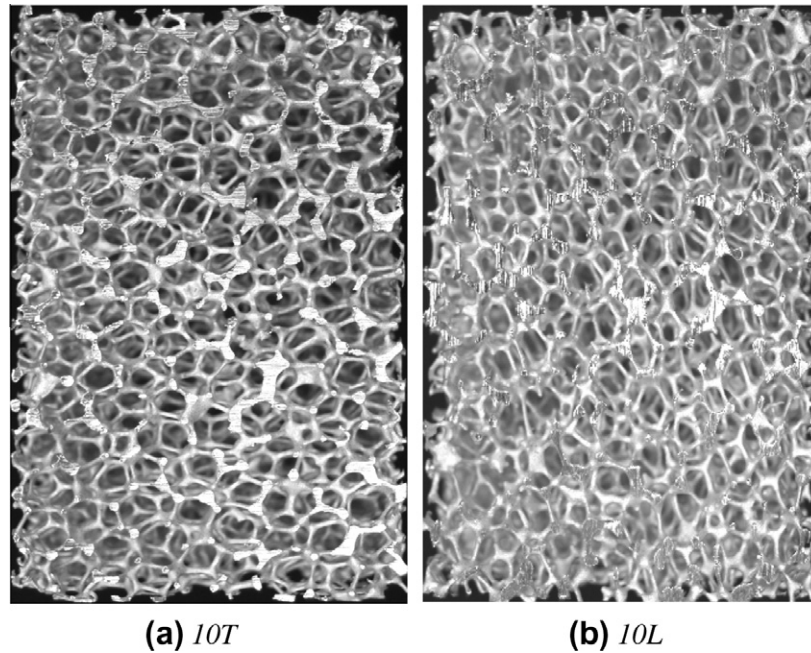
Fig. 1. Photographs of two undeformed 10PPI Duocel specimens (40 × 60 mm) sectioned along their mid plane where their constituent cells have its (a) smallest and (b) largest principal dimension aligned to the vertical loading axis.
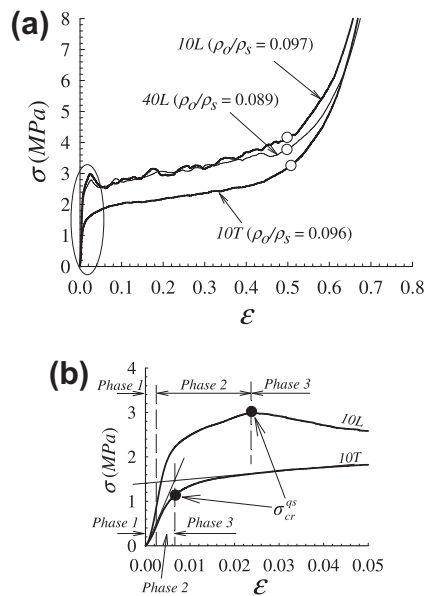

Fig. 2. (a) Typical nominal stress-strain curve for the foams. An open circle marks the point of densification in each curve. (b) Early deformation response of the 10L and 10T specimens.

Examination of partially crushed longitudinal specimens suggests that the cells collapse occurs in a 'shear-type' mode. This leads to a decrease in the global stiffness that result in a maximum load followed by a subsequent plastic loading path with a negative slope as seen in Fig. 2(b). This is responsible for the Type II behaviour under dynamic deformation, see *T–L*. By contrast, cells in the 10T specimens deform in a spatially, more uniform manner and in a symmetric mode which is consistent with the monotonic response seen in Phase 3. Our experiments confirm the results of numerical simulations of fully periodic, open-cell Kelvin foams by Gong et al. (2005a,b).

3.2. Quasi-static properties

Foams collapse plastically when the bending moment in the cell walls reaches the fully plastic moment. This gives a stress-strain curve with a plateau at the plastic collapse stress. However the curves in Fig. 2(a) are, strictly speaking, not perfectly plastic; hence, two stress values, viz. plastic collapse (or initial crushing) stress σ_{cr}^{qs} and plateau stress σ_{pl}^{qs}, are used to describe the quasi-static behaviour of the material. However, depending on the phenomena to be discussed, because of the relatively simple global response, the material is often simply characterised by just two quasi-static parameters, plateau stress and densification strain, for example in Gibson and Ashby (1997). This is the case when discussing the simple 'shock' theory (a two-parameter rigid, perfectly-plastic, locking, or *r–p–p–l*, model) for impact response as will be discussed in Section 4. However, unlike in Gibson and Ashby (1997), herein a distinction is made between these two stresses for reasons that will become clear later. Note that the superscript *qs* denotes quasi-static properties.

The plastic collapse stress σ_{cr}^{qs} of the 10L and 40L specimens corresponds to the first peak that separates Phases 2 and 3 in Fig. 2(b). This stress for the 10T specimens is found by a graphical construction illustrated in Fig. 2(b). Its corresponding strain is denoted by ε_{cr}. The densification strain – defined as the nominal strain value at which opposing walls in every cells come into contact and crush together – is extracted from each stress-strain curve using the 'efficiency' technique developed by Tan et al. (2002, 2005a). The data are then fitted to an empirical expression for the densification strain, the form of which is given by Ashby et al. (2000), as follows:

$$\varepsilon_D = 0.70\left[1 - 1.50(\rho_o/\rho_s) - 143.14(\rho_o/\rho_s)^3\right]. \tag{1}$$

To extract a plateau stress σ_{pl}^{qs}, the strain axis of the nominal stress-strain curve is first converted to time using

$$t = \varepsilon \cdot l_o/\dot{\delta}, \tag{2}$$

where compression was carried out at a constant rate of $\dot{\delta} = 45\ \mu ms^{-1}$. The plateau stress σ_{pl}^{qs} is defined as the time average value of the corresponding stress-time curve $\sigma_c(t)$ given by

$$\sigma_{pl}^{qs} = \langle \sigma_c \rangle \equiv \frac{1}{(t_D - t_{cr})} \int_{t_{cr}}^{t_D} \sigma_c(t)dt, \quad (3)$$

where t_{cr} and t_D is related to ε_{cr} (strain corresponding to the plastic collapse stress) and ε_D (densification strain), respectively, through Eq. (2). If the foam response is perfectly plastic, Eq. (3) gives $\sigma_{pl}^{qs} = \sigma_{cr}^{qs}$ as required. Fitting the data to the scaling law for the plastic collapse strength of open cell foams (Gibson and Ashby, 1997) in Fig. 3 gives:

In the longitudinal direction (for the 10L & 40L specimens):

$$\sigma_{cr}^{qs}/\sigma_{ys} = C_1(\rho_o/\rho_s)^{3/2} = 0.606(\rho_o/\rho_s)^{3/2}, \quad (4)$$

and

$$\sigma_{pl}^{qs}/\sigma_{ys} = C_2(\rho_o/\rho_s)^{3/2} = 0.708(\rho_o/\rho_s)^{3/2}, \quad (5)$$

and in the transverse direction (for the 10T specimens):

$$\sigma_{cr}^{qs}/\sigma_{ys} = C_3(\rho_o/\rho_s)^{3/2} = 0.323(\rho_o/\rho_s)^{3/2}, \quad (6)$$

and

$$\sigma_{pl}^{qs}/\sigma_{ys} = C_4(\rho_o/\rho_s)^{3/2} = 0.481(\rho_o/\rho_s)^{3/2}. \quad (7)$$

The scatter of the plastic collapse and plateau stresses (note that these are the non-normalised stresses) with respect to their mean values is approximately ±5% and ±10%, respectively.
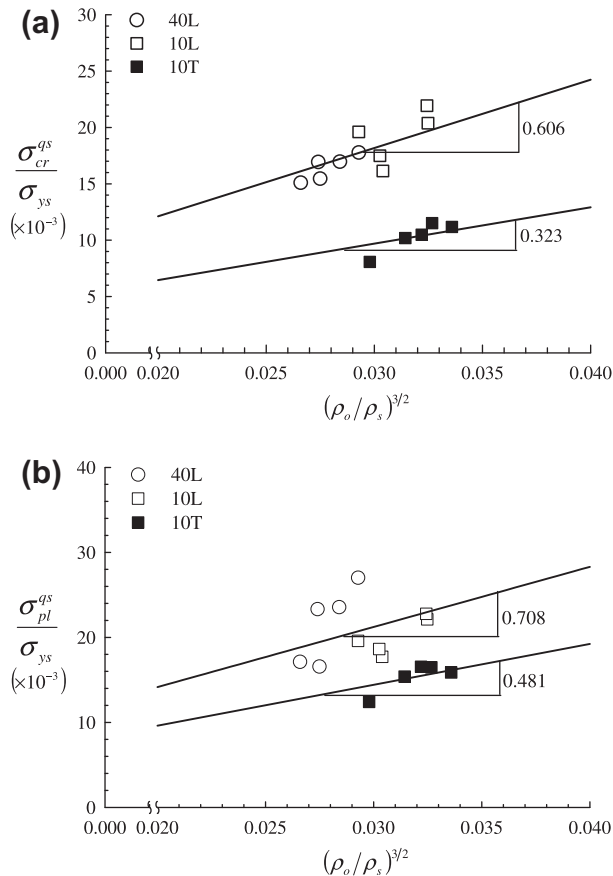

Fig. 3. Data for the quasi-static (a) plastic collapse and (b) plateau stresses (normalised by the yield strength of the ligaments) plotted against relative density $(\rho_o/\rho_s)^{1.5}$. The solid lines are the scaling relation in Eqs. (4)–(7).

4. Dynamic compression

Direct-impact tests were carried out on the foam projectiles which were fired axially against the end a silver-steel pressure bar at impact velocities V_i of up to 210 ms^{-1}. The details of the experimental procedure and the inverse method used in the indirect measurement of the impact forces are given in Tan et al. (2002), T–L, Tan (2005) and Inoue et al. (2001).

4.1. Force pulses and deformation patterns

Typical force pulses measured at different impact velocities are shown in Fig. 4. The time and nominal strain axes are linearly related to each other through Eq. (2) (replacing $\dot{\delta}$ with the impact velocity V_i) although this is, strictly speaking, only achieved with a high mass ratio – defined as the ratio of the mass of the backing plate to that of the foam specimen – of $M_r > 100$ (Tan, 2005; T–L). The complete details of the test programme can be found in Tan (2005). If the duration of the force pulse (total time required for the specimen to reach densification) is greater than the pressure bar transit time, then the pulse is truncated by reflected waves as seen in Fig. 4(a) and (d). In general, deformation occurs in three distinct phases as indicated in Fig. 4(c): a peak deceleration phase (I); a crushing phase (II); and, a densification phase (III) which are analogous to the elastic, plateau and densification regimes in Fig. 2(a). Note that Phase II deformation is *always* accompanied by a load drop, a feature absent in the 10T foams under quasi-static compression.

Two distinct types of deformation pattern (see Fig. 5) were observed depending on whether a critical velocity (to be discussed in Section 4.3) is exceeded. This critical velocity delineates the two distinct deformation patterns as follows:

(1) At *sub-critical* velocity compression. Fig. 5(a) shows a partially crushed specimen that has insufficient energy to achieve full crushing. Its deformation pattern is similar to that seen during quasi-static compression. Plastic collapse initiates at the weakest band of cells, almost always in the interior of the specimen, because the cells at the impact surface are reinforced by friction through their contact with the anvil which makes geometric softening much harder for them (Tan, 2005). Hence, plastic collapse of the cells at the impact surface only occurs in the latter stages of Phase II. In general, overall shortening of the specimens under sub-critical velocity compression is achieved by the accumulation of discrete, non-contiguous bands of crushed cells. This leads to a somewhat diffused deformation pattern wherein layers of crushed cells are separated by materials which survive without crushing if the foam is unloaded before reaching Phase III.

(2) At *super-critical* velocity compression. The specimen in Fig. 5(b) had no backing mass ($M_r = 0$) which is similar to a Taylor bullet-type test. On impact, the continuous transit of an elastic-plastic wave in the rear portion of the specimen reflected between the crush front and the rear end eventually brings the specimen to rest after many traversals in the rear part of the specimen. Cells at the impact surface undergo rapid plastic collapse and densify, the residual momentum is then transferred to an adjacent layer of cells, in a 'domino-type' effect where cell crushing occurs sequentially, in a planar manner, along the axis of the specimen. This occurs irrespective of whether the cell deformation mechanism is stable or not. With reference to the initial un-deformed configuration of the specimen, a planar interface, separating the crushed and the uncrushed cells,
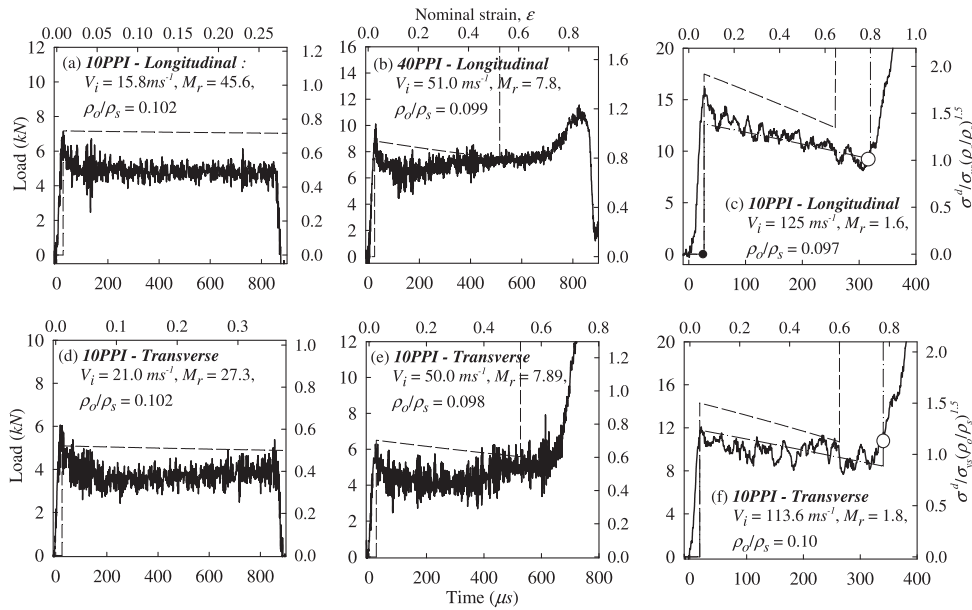
Fig. 4. Typical dynamic force pulses (solid lines) measured along the longitudinal (a–c) and transverse (d–f) directions. The theoretical predictions are plotted as dotted lines. The dash-dot line in (c) and (f) are theoretical prediction using the densification strain from the dynamic force pulse measured.
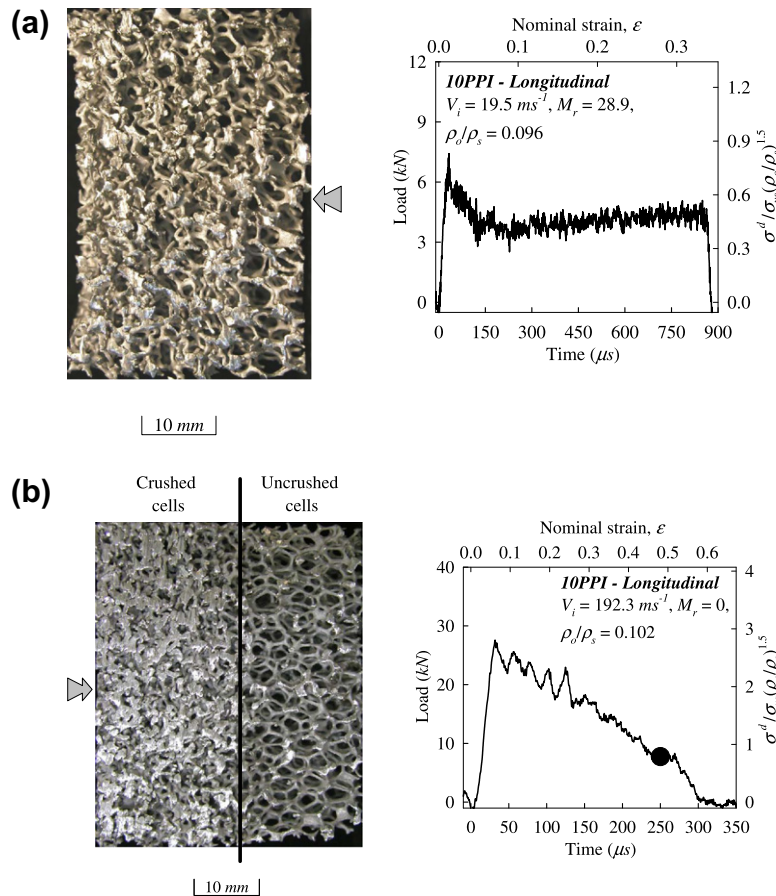

Fig. 5. Typical deformation pattern and their corresponding force pulse for a (a) 10L specimen under sub-critical velocity compression and (b) a 10L specimen (with specimen gauge length of 100 mm) under super-critical velocity compression. The arrow head denotes the impact end.

of approximately one cell-width (also, called the crush front), propagates along the specimen axis with time. This is also seen in the high-speed photographic images of Lee et al. (2006) and Radford et al. (2005). Because unloading from partially compacted states involves only a small elastic recovery, the interface remains visible in the fully

unloaded specimen in Fig. 5(b). Since the particle velocity and the deformation gradient (strain) in the specimen suffer rapid, finite changes across the crush front, it is idealised as a steady 'shock' wave or a first-order singular surface (Eringen and Şuhubi, 1974) across which the Rankine–Hugoniot relations must hold. A typical force pulse consists of successive decreasing peaks with time, reminiscent of the results of simulations of a heuristic spring-mass model by Shim et al. (1990). The decreasing peak forces are due to the decreasing momentum flux at the 'shock' front with time. If all the cells in the specimen have collapsed before the energy is fully dissipated, cell wall compression will occur if $M_r > 0$ which is reflected in the rapidly stiffening régime of Phase III. Otherwise, Phase III is absent from the force pulse as seen in Fig. 5(b). The point at which the specimen starts to unload is estimated by momentum considerations and is indicated by a solid circle in Fig. 5(b).

The critical velocity corresponding to a transition in the deformation pattern is estimated later.

4.2. Discussion of experimental results

Key material properties, see Tan (2005) for details, were extracted from each measured force pulse using techniques which parallel that for the quasi-static stress-strain curve. To account for density variations between test specimens, the data are normalised by the factor $(\rho_o/\rho_s)^{3/2}$. The same criterion used by Deshpande and Fleck (2000), where the dynamic strength is said to be enhanced if it exceeds the quasi-static scatter in strength, has been adopted here. The stress ratio Π, defined as the ratio of the dynamic to the corresponding quasi-static stress value, is also shown in the summary-figures (Figs. 6 and 7).

4.2.1. Plastic collapse stress

The normalised plastic collapse stress $\sigma_{cr}^d/(\rho_o/\rho_s)^{3/2}$ is plotted against impact velocity in Fig. 6. Significant enhancement of the plastic collapse strength is seen in *both* directions of the anisotropic foam with reference to its quasi-static strength. However, a greater plastic collapse strength enhancement is measured in foams compressed along the L direction for each impact velocity. Deshpande and Fleck (2000) estimated that the strain rate in the cell ligaments is an order of magnitude lower than its nominal strain rate $\dot{\varepsilon}$. Since the latter is less than 5000 s^{-1} in our tests, we conclude that rate sensitivity of the ligaments is negligible and that inertial/velocity sensitivity is the dominant effect. Microinertia of the ligaments causes a delay in triggering a buckling collapse mode and/or from the generation of an alternative less complaint cell collapse mechanism than that occurring in quasi-static compression. Finite elements simulations of the dynamic in-plane compression of regular honeycombs have established that the rotational and translational inertia of the ligaments are responsible for these effects (Hönig and Stronge, 2002). Here, the experimental data for the 3D foams also support the contention that inertial/velocity sensitivity is the most dominant.

For sub-critical impact velocities, the data in Fig. 6 are *approximately linear* with impact velocity. They suggest that the plastic collapse stress may be controlled by plastic compression of the ligaments before bending deformation predominates. If, for instance, the aluminium alloy cell wall material has a 'bi-linear' stress-strain relation, this wave travels at the plastic wave speed of

$$C_p \equiv \sqrt{E_p/\rho_s}. \tag{8}$$

where E_p is the plastic modulus. Since $E_p \approx 70.5$ MPa for Al6106–T6, giving a plastic wave speed C_p of approximately 161.6 ms^{-1}. Hence,
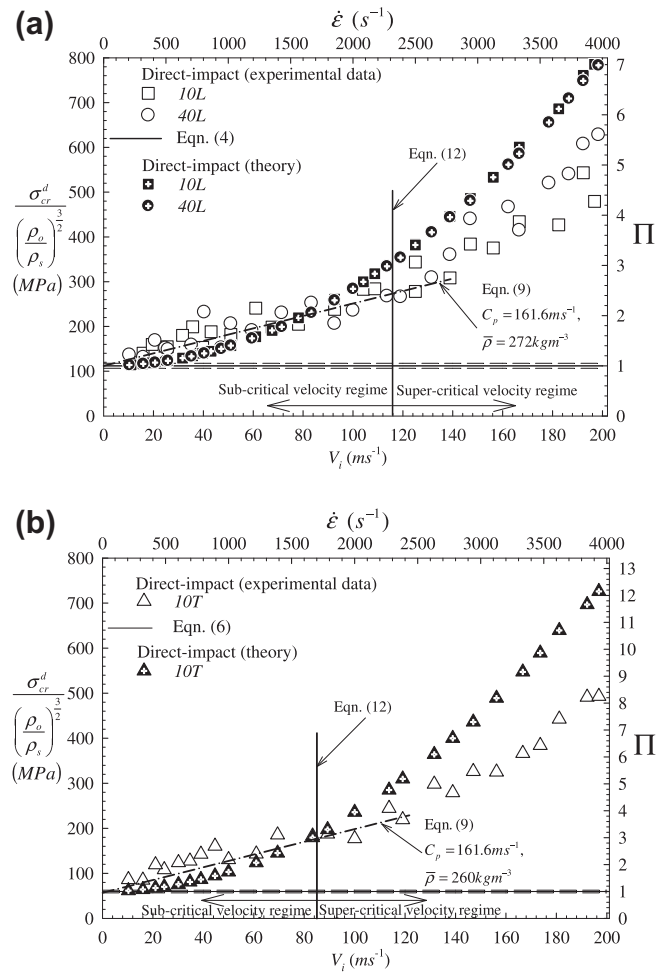

(a)

(b)

Fig. 6. Comparison between theory and experiment for the normalised plastic collapse stress for Duocel® foams with the (a) largest and (b) smallest dimension of their constituent cells parallel to the axis of compression. Dashed lines indicate corresponding quasi-static scatter in loads and $\dot{\varepsilon}$ is the nominal engineering strain rate.

the plastic collapse stress must vary linearly with impact velocity according to

$$\sigma_{cr}^d = \sigma_{cr}^{qs} + \bar{\rho}C_p V_i, \tag{9}$$

where $\bar{\rho} = \sum_N(\rho_o)_N/N$ is the average density of the N specimens tested. Eq. (9) fits the experimental data reasonably well, in particular, at the lower velocities. Calladine and English (1984) correctly described this phenomenon as a 'velocity' rather than a (nominal) strain-rate effect. An alternative (three-parameter) model has recently been investigated by Zheng et al. (2012), giving qualitatively similar sub-critical linear variations of the dynamic crushing strength with increasing impact velocity. This will be further discussed in Section 4.3.

4.2.2. Plateau stress

The plateau stress in Phase II – defined as the time averaged value of the force pulse divided by the cross-sectional area of the undeformed specimen A_o – is associated with the accumulation of bands of crushed cells. Variation of the normalised plateau stress $(\sigma_{pl}^d/(\rho_o/\rho_s)^{3/2})$ with impact velocity is shown in Fig. 7. Note that the superscript d denotes dynamic properties. The data have an *approximately quadratic* dependence on the impact velocity. The difference between the plastic collapse and the plateau stress increases with impact velocity, with the former being the higher of
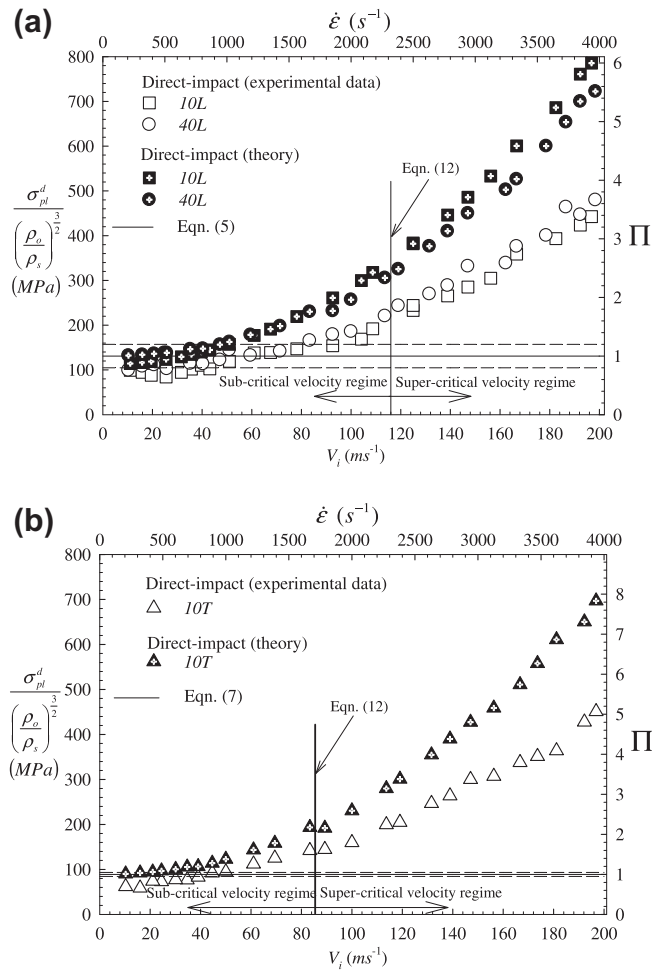
Fig. 7. Comparison between theory and experiment for the normalised plateau stress with the (a) largest and (b) smallest dimension of their constituent cells parallel to the axis of compression. Dashed lines indicate corresponding quasi-static scatter in loads and $\dot{\varepsilon}$ is the nominal engineering strain rate.

the two values, compare Figs. 6 and 7. At lower velocities the plateau stress is less than its corresponding quasi-static value probably because of the effect of internal elastic wave reflections although the reason is as yet unclear. The data shows that, in general, the dynamic plateau stress is insensitive to velocity below the values of 80 ms^{-1} and 50 ms^{-1} in the longitudinal and transverse directions, respectively. It is noteworthy that the variations of the two characteristic stresses with impact velocity are consistent with the recent treatment of 'transitional' and 'shock' modes in Zheng et al. (2012).

4.3. Comparison with results of one-dimensional shock model

By an analogy of a one-dimensional steady 'shock', using a thermo-mechanical approach, T–L derived dynamic properties of the foams based on a rate-independent r–p–p–l idealisation of its quasi-static stress strain curve. The predictions of this 1D 'shock' model will now be compared with the experimental data in the present study.

Within the limits of the r–p–p–l material idealisation, the predictions of the 'shock' model compare well with the experimental force-time pulses as shown in Fig. 4. Although the two-parameter 'shock' model is not applicable at sub-critical velocities (see Section 4.1 and the discussion to follow), a reasonable agreement with the force pulses is seen. In general, the theory does not reliably

predict the onset of densification because the actual foam material is not perfectly rigid at its densification strain. The extent to which the material behind the 'shock' is compacted depends on the impact velocity and the compact material may have a nominal strain greater than the nominal densification strain value given by Eq. (1). The discrepancy between the predicted and experimental force pulses, especially at the higher impact velocities, is believed to be a consequence of this and will be addressed in the Section 4.4. By using an adjusted densification strain value (indicated by a hollow circle) from the experimental force pulse in the calculations, an excellent agreement with the experiment, see Fig. 4(c) and (f), which supports the argument that, in T–L and elsewhere, the assumption of a constant densification strain is too crude. A better agreement between theory and experiment should, in general, be achieved by relaxing/modifying the locking assumption at the densification strain.

The theoretical 'shock-enhanced' plastic collapse stress was found in Tan (2005) and in T–L to be:

$$\sigma_{cr}^d = \sigma_{cr}^{qs} + \rho_o V_i^2 / \varepsilon_D. \tag{10}$$

Fig. 6 shows that the two-parameter shock theory consistently under-predicts the plastic collapse strength of the foams in the sub-critical velocity régime but tends to over-predict in the super-critical velocity régime; this is irrespective of the direction which the anisotropic foam is compressed. At sub-critical velocities, the 'shock' model underestimates the plastic collapse stress due to microinertia effects and the plastic wave model, viz. Eq. (9) or Zheng et al. (2012), should be used instead. This shows that the dynamic response of the foams during an impact (non-zero initial velocity) process exhibits typical Type-II structural characteristics (Calladine and English, 1984), irrespective of the form of their quasi-static force-displacement curve; compare, for example, with the 10T specimens. By analogy with the previous work on 0° wood specimens (Reid et al., 1993), one can argue that the plastic collapse stress will increase more substantially than the 'shock' theory can predict.

The theoretical dynamic plateau stress is defined as the time average value of dynamic stress-time pulse, $\sigma^d(t)$, given by Tan (2005) and T–L as

$$\sigma_{pl}^d = \langle \sigma^d \rangle = \frac{1}{t_D} \int_0^{t_D} \sigma^d(t) dt, \tag{11}$$

where t_D corresponds to the time where rigid locking of the whole of the foam specimen has occurred. The values obtained using Eq. (11) are plotted against impact velocity alongside the corresponding experimental data in Fig. 7. The consistent over-prediction of the plateau stresses by the model are due to two reasons: the first is possibly due to the effects of internal wave reflection in the foam material which is not considered in the 'shock' model and the second is due to the higher levels of strain achieved experimentally than are possible analytically when using the simplified two-parameter r–p–p–l material model. As previously shown, if the adjusted densification strain (indicated by a hollow circle) of the dynamic force pulse were used in the calculations, then an excellent agreement with the experiment data can be achieved.

As previously discussed, a switch in deformation pattern from discrete crush band multiplication to progressive cell crushing occurs when the impact velocity exceeds a critical value. It was conjectured by Reid and Peng (1997) that sequential cell crushing occurs when the kinetic energy of a band of collapsing cells crosses a critical energy barrier. Using a thermo-mechanical formulation, the kinematic existence condition for continuing 1D steady 'shock' propagation in an r–p–p–l foam rod by Tan (2005) and T–L produced a similar result, expressed as

$$V_{cr} = (2C_n\sigma_{ys}/\rho_s)^{1/2}(\rho_o/\rho_s)^{1/4}\varepsilon_D^{1/2}, \tag{12a}$$

where the subscript $n = 1$ (10L and 40L) or 3 (10T). The predicted critical velocity using Eq. (12a) is 116 ms^{-1} (using $\rho_o/\rho_s = 0.1$) and 85 ms^{-1} (using $\rho_o/\rho_s = 0.096$) for compression along the longitudinal and transverse directions which agrees reasonably well with the experimental data of 110 ms^{-1} and 70 ms^{-1}, respectively (see Figs. 6 and 7).

An alternative approach, recently described in Zheng et al. (2012), leads to the simple theoretical formula:

$$V_{cr} = C_p\varepsilon_D, \tag{12b}$$

where C_p, unlike that in Eq. (9), is the wave speed based upon the slope of the 'plateau' region in the stress strain curve, now taken as having a non-zero value (as distinct to the two-parameter r–p–p–l model, with its perfectly plastic plateau assumption). Zheng et al. (2012) formulation is based on a three-parameter rigid, linearly strain hardening, locking (r–l–sh–l) model using continuum wave theory in which the response is either in the 'transitional mode' or the 'shock mode'. The latter is essentially the same as the simple shock theory under discussion herein. Their model allows the lower impact velocity scenarios to be examined, see Zheng et al. (2012). Using Eq. (12b), the critical impact velocities for the 10L and 40L specimens discussed herein are between 57 and 60 ms^{-1} and for the 10T specimens 57 ms^{-1}, these values depending on the density of the foam. An interesting observation on this approach, from a design perspective, is that the results presented in Figs. 6 and 7 bear out the linear and quadratic dependence of the crush stress with impact velocity variations observed in the tests on Duocel® specimens discussed herein.

4.4. Effect of ε_D on the accuracy of the one-dimensional shock model

The r–p–p–l material definition is based on the quasi-static nominal stress-strain curve. Furthermore, the locking (densification) strain defines the onset of densification in this quasi-static curve in this model. For this reason, the r–p–p–l model will over-estimate stresses (according to Eq. (10)) and under-estimate strains with increasing impact velocity. Clearly, improved predictions can be made by combining the "shock" theory with a somewhat more accurate material description, for example with a non-linear hardening stress-strain curve as employed by Pattofatto et al. (2007), Harrigan et al. (2005) and Harrigan et al. (2010). Note that the closed form solution in Pattofatto et al. (2007) corresponds to the "shock" theory whereas the FE predictions do not. A discussion on this is provided in Harrigan et al. (2010).

Other researchers have considered a wider range of impact velocities and have taken appropriate regions from the stress-strain curve for predictions at different impact velocities (Lopatnikov et al., 2003). Even for the quasi-static nominal stress-strain curve, the non-linear stages in both the early and late part of the deformation would have some effect, see for instance the stages of the stress-strain curve defined in da Cunda et al. (2011). It would appear that the deformation mode can be a function of impact velocity (as shown in Zou et al., 2009), there the densification strain was estimated from the finite-element data for comparison with quasi-static values rather than predicted by them. The material properties that are needed to predict the shock compression of cellular materials are ill-defined (Harrigan et al., 2010). "Equations of state" for solid materials are normally derived from plate-impact test data. Equivalent data for compaction waves in cellular materials are not available due to the difficulties associated with measuring the "states" on either side of a compaction wave, though an attempt to do this in the context of, necessarily, low-velocity SHPB tests is discussed in Section 4 of the paper by Elsinari et al. (2007).

Currently, quasi-static stress–strain curves are used to predict stresses under impact loading conditions. These quasi-static material properties are usually measured over length scales within which several cells are present in any direction and deformation modes are very different from those during dynamic compaction. Clearly, as in the 2D study of Zou et al. (2009), under dynamic loads the cells at the deformation front are compelled to deform to greater levels. For this paper, we discuss the implications of and evidence for this behaviour relevant to 3D foams in the context of the simple two-parameter shock theory. Specifically these imply that the 'effective densification strain' at the shock front is velocity dependent.

The numerical simulations of the in-plane dynamic crushing of 2D hexagonal honeycombs by Zou et al. (2009) have shown that the 'densification strain' increases with crushing velocity and asymptotes to a limit once a shock front develops as shown in Fig. 8 taken from Zou et al. (2009). It is hypothesized that the same is also true for the 3D Duocel® foams studied here. To test this hypothesis, Eq. (10) is re-arranged to give

$$\varepsilon_D = \rho_o V_i^2/(\sigma_{cr}^d - \sigma_{cr}^{qs}), \tag{13}$$

where σ_{cr}^d is the plastic collapse stress measured experimentally and σ_{cr}^{qs} is from Eqs. (4)–(7) (the choice of which depends on the cell size and direction of compression). Fig. 9 shows the variation of the 'effective' densification strain ε_D with impact velocity V_i. The densification strain predicted using Eq. (1) is plotted in the same figure for comparison. Although the data shows considerable scatter due to the variability of the 3D Duocel® foams, a trend similar to that seen in numerical simulations by Zou et al. (2009) is observed. Therefore, it is not unreasonable to conclude that a higher level of densification strain at the shock front must have been achieved experimentally with increasing impact velocity in 3D foams than that assumed when using the simplified r–p–p–l material model or the three-parameter model of Zheng et al. (2012). This is the main reason of over-prediction by the shock theory at increasing impact velocities seen in Figs. 6 and 7.

To better-model this complex behaviour, one may require a dynamic version of the study by Bardenhagen et al. (2005) and Brydon et al. (2005) using HPC facilities, essentially a micromechanics simulation. This would contradict the conclusions of Pattofatto et al. (2007) that more refined microstructural models are not required. Alternatively, if one wishes to retain a continuum mechanics approach, one would essentially have to repeat the study in Zheng et al. (2012), recognising that a two-mode model with a velocity
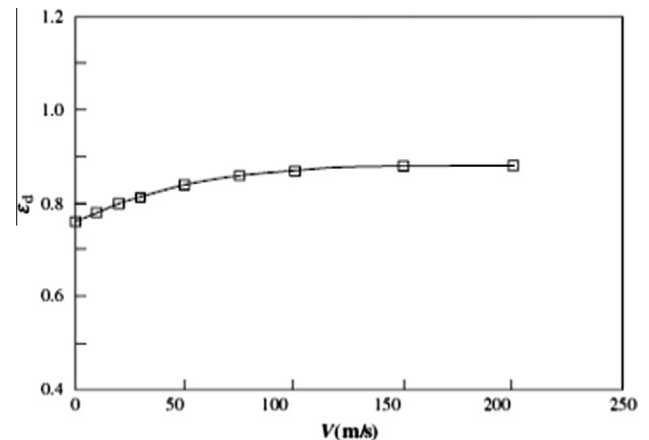

Fig. 8. Densification strains of the honeycomb under different crushing velocities (cells compressed in the X_1 direction) – taken from Zou et al. (2009).
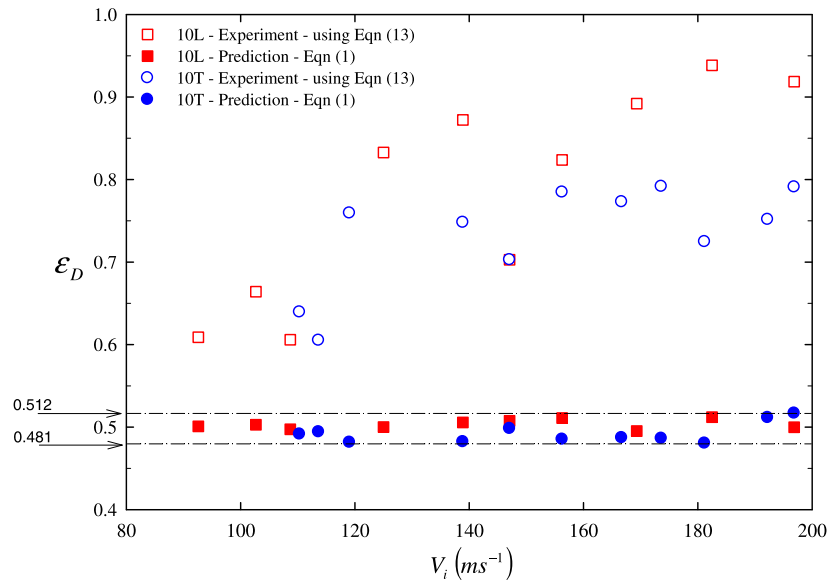
Fig. 9. Comparison between the densification strains predicted using Eq. (1) and that deduced from the experimental data using Eq. (13).

dependent densification strain at the shock front. This issue will be the subject of future research.

5. Conclusions

Significant enhancement of the plastic collapse stress is measured in both the sub-critical and super-critical velocity régimes in experiments using Duocel® foams. In the sub-critical regime, translational and, to a lesser extent, rotational inertia of the cell walls, rather than 'shock' propagation, are responsible for the strength enhancement. They introduce an initial phase to the deformation, which is dominated by plastic axial compression of the cell walls. The linear variation of the plastic collapse strength data with impact velocity and the good agreement with the predictions of a one-dimensional plastic wave theory support the influence of Type-II microinertia effects. In the super-critical velocity régime, the data for the plastic collapse stresses varies with the square of impact velocity which is consistent with 'shock' propagation. The plateau strength data is relatively insensitive to the impact velocity in the sub-critical régime for both foams. Significant enhancement of the plateau stress is observed in the super-critical velocity régime where 'shock' propagation effects are important. The increasing discrepancies between the prediction by the shock theory was due to the higher level of densification strain that can be achieved experimentally than is predicted analytically when using the simple theories, implying the need to incorporate further micromechanical features, essentially incorporating the velocity-dependence of the shock front densification strain.

Acknowledgements

References

Ashby, M.F., Evans, A.G., Fleck, N.A., Gibson, L.J., Hutchinson, J.W., Wadley, H.N.G., 2000. Metal Foams: A Design Guide. Butterworth Heinemann, Oxford.

Bastawros, A., Baart-Smith, H., Evans, A.G., 2000. Experimental analysis of deformation mechanisms in a closed-cell aluminium alloy foam. J. Mech. Phys. Solids 48, 301–322.

Bardenhagen, S.G., Brydon, A.D., Guilkey, J.E., 2005. Insight into the physics of foam densification via numerical simulation. J. Mech. Phys. Solids 53, 597–617.

Brydon, A.D., Bardenhagen, S.G., Miller, E.A., Seidler, G.T., 2005. Simulation of the densification of real opened-cell foam microstructures. J. Mech. Phys. Solids 53, 2638–2660.

Calladine, C.R., English, R.W., 1984. Strain-rate and inertia effects in the collapse of two types of energy-absorbing structure. Int. J. Mech. Sci. 26, 689–701.

da Cunda, L.A.B., Oliveira, B.F., Creus, B.F., 2011. Plasticity and damage analysis of metal foams under dynamic loading. Materialwiss. Werkst. 42 (5), 356–364.

Deshpande, V.S., Fleck, N.A., 2000. High strain rate compressive behaviour of aluminium alloy foams. Int. J. Impact Eng 24, 277–298.

Elsinari, I., Pattofatto, S., Zhao, H., Tsitsiris, H., Hild, F., Girard, Y., 2007. Shock enhancement of cellular structures under impact loading: part I. Experiments. J. Mech. Phys. Solids 55, 2652–2671.

Eringen, A.C., Şuhubi, E.S., 1974. Elastodynamics. Finite Motions, vol.1. Academic Press, New York.

Gibson, L.J., Ashby, M.F., 1997. Cellular Solids: Structure and Properties, second ed. Cambridge University Press, Cambridge.

Gong, L., Kyriakides, S., 2005a. Compressive response of open-cell foams. Part II: initiation and evolution of crushing. Int. J. Solids Struct. 42, 1381–1399.

Gong, L., Kyriakides, S., Jang, W.J., 2005b. Compressive response of open-cell foams. Part I: morphology and elastic properties. Int. J. Solids Struct. 42, 1355–1379.

Harrigan, J.J., Reid, S.R., Tan, P.J., Reddy, T.Y., 2005. High rate crushing of wood along the grain. Int. J. Mech. Sci. 47, 521–544.

Harrigan, J.J., Reid, S.R., Yaghoubi, S.A., 2010. The correct analysis of shocks in a cellular material. Int. J. Impact Eng 37, 918–927.

Hönig, A., Stronge, W.J., 2002. In-plane dynamic crushing of honeycomb – part I: crush band initiation and wave trapping. Int. J. Mech. Sci. 44, 1665–1696.

Inoue, H., Harrigan, J.J., Reid, S.R., 2001. A review on inverse analysis for indirect measurement of impact force. ASME Appl. Mech. Rev. 54, 503–524.

Lee, S., Barthelat, F., Moldovan, N., Espinosa, H.D., Wadley, H.N.G., 2006. Deformation rate effects on failure modes of open-cell Al foams and textile cellular materials. Int. J. Solids Struct. 43, 53–73.

Lopatnikov, S.L., Gama, B.A., Haque, M.J., Krauthauser, C., Guden, M., Hall, I.W., 2003. Dynamics of metal foam deformation during Taylor cylinder–Hopkinson bar impact experiment. Comput. Struct. 61, 61–71.

Montanini, R., 2005. Measurement of strain rate sensitivity of aluminium foams for energy dissipation. Int. J. Mech. Sci. 47, 26–42.

Pattofatto, S., Elsinari, I., Zhao, H., Tsitsiris, H., Hild, H., Girard, Y., 2007. Shock enhancement of cellular structures under impact loading: part II. Analysis. J. Mech. Phys. Solids 55, 2672–2686.

Radford, D.D., Deshpande, V.S., Fleck, N.A., 2005. The use of metal foam projectiles to simulate shock loading on a structure. Int. J. Impact Eng 31, 1152–1171.

Reid, S.R., Peng, C., 1997. Dynamic crushing of wood. Int. J. Impact Eng 19, 531–570.

Reid, S.R., Reddy, T.Y., Peng, C., 1993. Dynamic compression of cellular structures and materials. In: Jones, N., Wierzbicki, T. (Eds.), Structural Crashworthiness and Failure. Elsevier Applied Science Publishers, pp. 295–340.

Shim, V.P.W., Tay, B.Y., Stronge, W.J., 1990. Dynamic crushing of strain softening cellular structures – a one-dimensional analysis. J. Eng. Mater. Technol. Trans. ASME 112, 398–405.

Tan, P.J., 2005. Dynamic mechanical properties of metal foams. Ph.D. Thesis. The University of Manchester, UK.

Tan, P.J., Harrigan, J.J., Reid, S.R., 2002. Inertial effects in the uniaxial dynamic compression of a closed-cell aluminium alloy foam. Mater. Sci. Technol. 18, 480–488.

Tan, P.J., Reid, S.R., Harrigan, J.J., Zou, Z., Li, S., 2005a. Dynamic compressive strength properties of metal foams. Part I – experimental data and observations. J. Mech. Phys. Solids 53, 2174–2205.

Tan, P.J., Reid, S.R., Harrigan, J.J., Zou, Z., Li, S., 2005b. Dynamic compressive strength properties of metal foams. Part II – 'shock' theory and comparison with experimental data and numerical models. J. Mech. Phys. Solids 53, 2206–2230.

Wang, Z., Ma, H., Zhao, L., Yang, G., 2006. Studies on the dynamic compressive properties of open-cell aluminium alloy foams. Scripta Mater. 54, 83–87.

Yi, F., Zhu, Z., Zu, F., Hu, S., Yi, P., 2001. Strain rate effects on the compressive property and the energy-absorbing capacity of aluminium alloy foams. Mater. Charact. 47, 417–422.

Yu, J.L., Li, J.R., Hu, S.S., 2006. Strain-rate effect and micro-structural optimization of cellular metals. Mech. Mater. 38, 160–170.

Zheng, Z., Liu, Y., Yu, J., Reid, S.R., 2012. Dynamic crushing of cellular materials: continuum-based wave models for transitional and shock modes. Int. J. Impact Eng 42, 66–79.

Zou, Z., Reid, S.R., Tan, P.J., Harrigan, J.J., Li, S., 2009. Dynamic crushing of honeycombs and features of shock fronts. Int. J. Impact Eng 36, 165–176.